Rare Metal Materials and Engineering
Volume 55, Issue 2, February 2026
Available online at www.rmme.ac.cn

Science Press

Cite this article as: Zhang Chong, Wang Xin, Xu Hailong, et al. Microstructure and Thermal Properties of $MoSi_2$ and $Gd_2Zr_2O_7$ Composite Coatings on Mo-Re Alloy[J]. Rare Metal Materials and Engineering, 2026, 55(02): 315-321. DOI: https://doi.org/10.12442/j.issn.1002-185X.20250091.

ARTICLE

Microstructure and Thermal Properties of $MoSi_2$ and $Gd_2Zr_2O_7$ Composite Coatings on Mo-Re Alloy

Zhang Chong, Wang Xin, Xu Hailong, Li Yanchao, Ma Tongxiang, Wang Shaopeng

Northwest Institute for Nonferrous Metal Research, Xi'an 710016, China

Abstract: Dual-layer thermal barrier coatings (TBCs) with ultrahigh temperature resistance were prepared on the surface of molybdenum-rhenium alloy hot-end components. The preparation of the $MoSi_2$-$Gd_2Zr_2O_7$ dual-layer TBCs was designed based on the coefficient of thermal expansion and the coating functionality, and it was completed using atmospheric plasma spraying technique. The microstructure, mechanical properties, and thermal properties were analyzed. Results indicate that the adhesion of the prepared dual-layer composite TBCs is excellent, and no noticeable cracks appear at the interface. Compared with the $MoSi_2$ coating with a low fracture toughness (0.88 $MPa \cdot m^{1/2}$), the $Gd_2Zr_2O_7$ coating exhibits higher fracture toughness (1.74 $MPa \cdot m^{1/2}$) and stronger resistance to crack propagation. The prepared $MoSi_2$-$Gd_2Zr_2O_7$ composite coatings have a high porosity (39%), low thermal conductivity (1.020 $W \cdot (m \cdot K)^{-1}$, 1200 °C), and low thermal diffusivity (0.249 mm^2/s, 1200 °C). Additionally, they possess a high oxygen-vacancy concentration, which ensures excellent insulation performance.

Key words: $MoSi_2$-$Gd_2Zr_2O_7$ coating; molybdenum-rhenium alloy; TBCs; thermal insulation performance

1 Introduction

Molybdenum-rhenium (Mo-Re) alloys are extensively used in aerospace, nuclear, and military applications due to their exceptional radiation resistance, high tensile strength, favorable flexibility, and robust thermal shock resistance[1]. They are usually used to fabricate engine nozzles, combustion chamber liners, and other critical military components[2–4]. To enable operation at ultrahigh temperatures (>1700 K), thermal barrier coatings (TBCs) must be applied to the alloy surface. However, the traditional plasma-sprayed yttria-stabilized zirconia (YSZ) coating can only be applied in working environments below 1400 K due to its phase transformation (t'→t+c)[5–7] at elevated temperatures. Consequently, it is essential to develop a heat-insulating coating material characterized by superior thermal insulation properties and a high phase transformation temperature to address the issue of low service temperatures for Mo-Re alloys.

Among the rare earth zirconates, gadolinium zirconate ($Gd_2Zr_2O_7$, namely GZ) exhibits a crocolite structure and demonstrates significant phase stability with the transition to a defective fluorite structure at 1550 °C. Additionally, its thermal conductivity is lower than that of YSZ[8–10]. However, the significant mismatch in the coefficients of thermal expansion between the coating and the substrate adversely affects the mechanical properties of the GZ coatings, leading to inadequate thermal shock resistance[11–13]. This restriction significantly hinders the high-performance application of the GZ coatings on Mo-Re alloys. Consequently, selecting an appropriate bonding layer with a coefficient of thermal expansion matching those of the substrate and top layer is essential.

The $MoSi_2$ coatings have high melting points, moderate density, and outstanding comprehensive performance[14–16].

Received date: February 24, 2025
Foundation item: Supported by Scientific and Technological Innovation of Shaanxi Provincial State-Owned Capital Operation Budget (2022-056); Institute's Self-Developed Technology Program (0801YK2317); Qin Chuangyuan Cites High-Level Innovation and Entrepreneurship Talent Program (QCYRCXM-2023-120); Qin Chuangyuan Industry Cluster Zone "Four Chains" Integration Program (2024CY-JJQ-46); National Natural Science Foundation of China (52071274); Key Research and Development Projects of Shaanxi Province (2023-YBGY-442); Science and Technology Nova Project-Innovative Talent Promotion Program of Shaanxi Province (2020KJXX-062)
Corresponding author: Zhang Chong, Master, Engineer, Northwest Institute for Nonferrous Metal Research, Xi'an 710016, P. R. China, Tel: 0086-29-86283410, E-mail: zhangchong0411@163.com; Wang Shaopeng, Ph. D., Professor, Northwest Institute for Nonferrous Metal Research, Xi'an 710016, P. R. China, Tel: 0086-29-86230194, E-mail: pengfly239@163.com

During high-temperature oxidation, the volatile oxidation product MoO_3 evaporates promptly, enabling the formation of a complete and continuous SiO_2 protective film on the surface of $MoSi_2$ which effectively inhibits oxygen diffusion[17–19]. Consequently, it is regarded as an up-and-coming candidate for high-temperature protective coatings[20–22]. Additionally, the coefficient of thermal expansion of $MoSi_2$ (9.2×10^{-6} K^{-1}) lies between that of the base Mo-Re alloy (7.5×10^{-6} K^{-1}) and the GZ coatings (10.4×10^{-6} K^{-1})[23–25] used in this study, allowing $MoSi_2$ to function simultaneously as an anti-oxidation coating and an adhesive phase for GZ.

This study adopted a coating design approach and employed atmospheric plasma spraying (APS) to fabricate $MoSi_2$-GZ coatings. The microstructure and performance of TBCs were characterized. This research is anticipated to offer valuable insights into the high-performance application of $MoSi_2$-GZ coatings on Mo-Re alloys.

2 Experiment

Mo-Re alloys with dimension of *Φ*25.2 mm×3 mm were obtained by wire-electrode cutting and then used as the substrates. $MoSi_2$ (powder provided by Beijing Sunspraying New Material Co., Ltd) coatings of about 50 μm in thickness were fabricated lay-by-layer on the substrate as bonding layers by APS (SG-100, Praxair S. T., America) with commercial powders. The information of $MoSi_2$ and $Gd_2Zr_2O_7$ powders is shown in Table 1. The top coating of $Gd_2Zr_2O_7$ (referred to as GZ, thickness of about 300 μm, powder provided by Beijing Sunspraying New Material Co., Ltd) was deposited via APS (SG-100, Praxair S.T., America) with the powder synthesized by solid-state reaction, as shown in Fig. 1. The deposition parameters were optimized using the Box-Behnken Design method[26], and the detailed spray parameters are shown in Table 2. According to the coating deposition process, the samples were heat-treated at 600 °C for 1 h in an argon atmosphere furnace to diminish the residual stress.

The cross-section morphology and element contents of the as-sprayed coatings were analyzed using scanning electron microscope (SEM, Hitachi SU5000, Japan) equipped with an energy-dispersive spectrometer (EDS, INCA-AE350). Phase composition was determined by X-ray diffractometer (XRD, SmartLab, Japan) with Cu-Kα radiation.

The coating microhardness was evaluated using Vickers indentation testing (HVS-1000) with a load of 200 g (≈2 N) and a dwell time of 15 s. The average microhardness was determined by repeating the measurement for 10 times and excluding the maximum and minimum values[27].

To measure the fracture toughness of GZ coatings, a Vickers indenter with a load of 1 N was used to create appropriate cracks on the polished cross-section of coatings[28]. According to the Evans & Wilshaw model, the fracture toughness could be calculated by Eq.(1)[29–30], as follows:

$$K_{IC} = 0.079\frac{P}{a^{3/2}}\lg\frac{4.5a}{c} \quad (1)$$

where K_{IC} is the fracture toughness (MPa·m$^{1/2}$), P is the load of the indenter (N), c is the length from the tip of the cracks to the center of indentation (m), and a is the half-length of the diagonal (m).

The porosity of the coatings was quantified through the analysis of SEM cross-section images using Image Pro Plus software. The bond strength of the coatings was evaluated through tensile tests based on GB/T 8642-2002 standard.

The specific heat capacity of $MoSi_2$-GZ coatings was measured by differential scanning calorimeter (DSC, LFA 467, NETZSCH, Germany), and the thermal conductivity and diffusivity were detected using free-standing samples with dimension of 10 mm×10 mm×1.19 mm.

3 Results and Discussion

3.1 Microstructure of $MoSi_2$-GZ coatings

The surface morphologies of the $MoSi_2$ bonding layer and the GZ top layer are shown in Fig. 2. The $MoSi_2$ layer is not polished to improve the bonding strength of the coating. The splashed droplets on the surface, lamellar stacking, and

Table 1 Information of $MoSi_2$ and $Gd_2Zr_2O_7$ powders

Powder	Size, D_{10}/μm	Size, D_{50}/μm	Size, D_{90}/μm	Loose specific mass/s·cm^{-3}	Powder fluidity/s·50 g^{-1}
$MoSi_2$	29.5	47.1	73.3	1.56	40.54
$Gd_2Zr_2O_7$	32.5	46.3	65.4	2.06	24.67

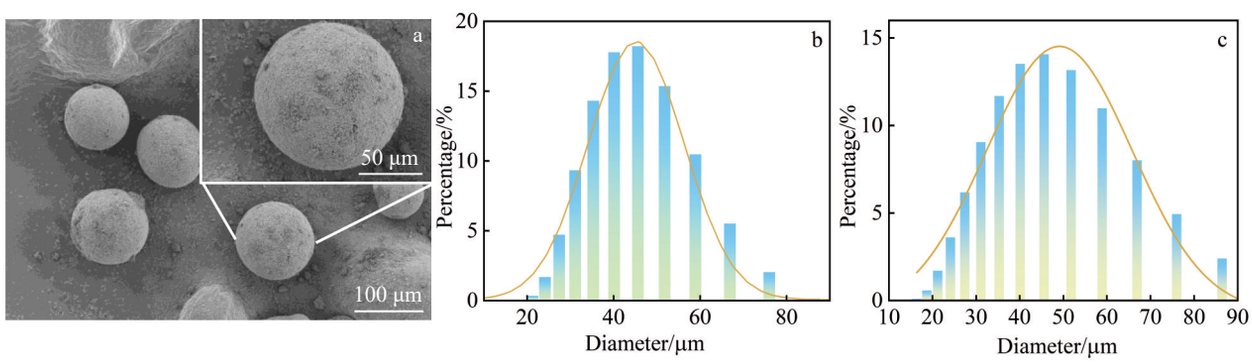

Fig.1 SEM image of GZ powder (a); granularities of $MoSi_2$ powder (b) and GZ powder (c)

Table 2 APS parameters of GZ top layer and $MoSi_2$ bonding layer

Parameter	Value	
	$MoSi_2$	GZ
Spray distance/mm	100	100
Primary gas (Ar) flow rate/L·min^{-1}	104	90
Second gas (H_2) flow rate/L·min^{-1}	3	4
Carrier Ar gas flow rate/L·min^{-1}	12	12
Voltage/V	40	45
Current/A	750	850
Powder feed rate/r·min^{-1}	2	2
Gun traverse speed/mm·s^{-1}	700	700

microcracks in the coating can still be observed. Although the layered characteristics of the GZ top layer are not obvious after surface polishing, pores within the coating remain visible.

The cross-section microstructures of the Mo-Re alloy surface coated with $MoSi_2$ and GZ layers are shown in Fig. 3. Fig. 3a presents the overall cross-section morphology of the coating. The overall thickness of the coating is approximately 350 μm with the $MoSi_2$ layer thickness of approximately 50 μm and the GZ layer thickness of 300 μm. It can be observed that the coatings are firmly bonded to the substrate, and no extensive horizontal/vertical cracks or peeling are present on the coating. As shown in the inset of Fig. 3a, the interface bonding at the contact region with the external surroundings remains excellent, and the microcracks may be attributed to the damage during wire-electrode cutting.

The porosity of the coating is 39%, as shown in Fig.3b. It is observed that a large-scale porous area and a small portion of semi-molten regions exist in the GZ top layer. At the semi-molten region, the internal structure is composed of columnar crystals formed through layered growth. This may be attributed to the incomplete heat input and untimely cooling during the spraying process[31]. Fig. 3c and 3d depict the interface between the GZ top layer and the $MoSi_2$ bonding layer and that between the bonding layer and the substrate, respectively. Microcracks (widths at the nanometer scale) can still be observed, and the defects, such as cracks, exist at the interfaces. As shown in Fig.3c, component segregation occurs in the $MoSi_2$ region. As listed in Table 3, the proportion of Mo at spots 3 and 4 in the $MoSi_2$ region is conspicuously higher than that at spot 2. Moreover, since the coatings undergo oxidation during the spraying process, it is highly likely that spots 3 and 4 are the enrichment zones of Mo oxides, and spot 2 is the area where $MoSi_2$ is oxidized[32]. This result also accounts for the phenomenon that no compositional segregation occurs in the substrate and bonding layer regions.

XRD patterns of the $MoSi_2$ and GZ coatings on Mo-Re alloy is shown in Fig.4, which manifest the orientation of the $MoSi_2$ and GZ grains and the intensity of the diffraction peaks after spraying. It can be seen that no conspicuous phase transition occurs during the preparation of the coatings. However, some regions become amorphous[33]. GZ surface layer is fabricated on the Mo-Re alloy surface without the interference of impurity phases.

3.2 Mechanical properties of $MoSi_2$-GZ coatings

The indentation morphologies of the $MoSi_2$-GZ composite coatings at various distances from the surface are shown in Fig. 5. Fig. 5d illustrates the indentation morphology of $MoSi_2$ coating. It can be observed that the cracks in GZ coating are shorter than those in $MoSi_2$ coating. The *c*/*a* ratios for GZ and $MoSi_2$ coatings are 1.57–2.04 and 3.25±0.22, respectively. The *c*/*a* ratio within the range of 0.6–4.5 indicates that the fracture

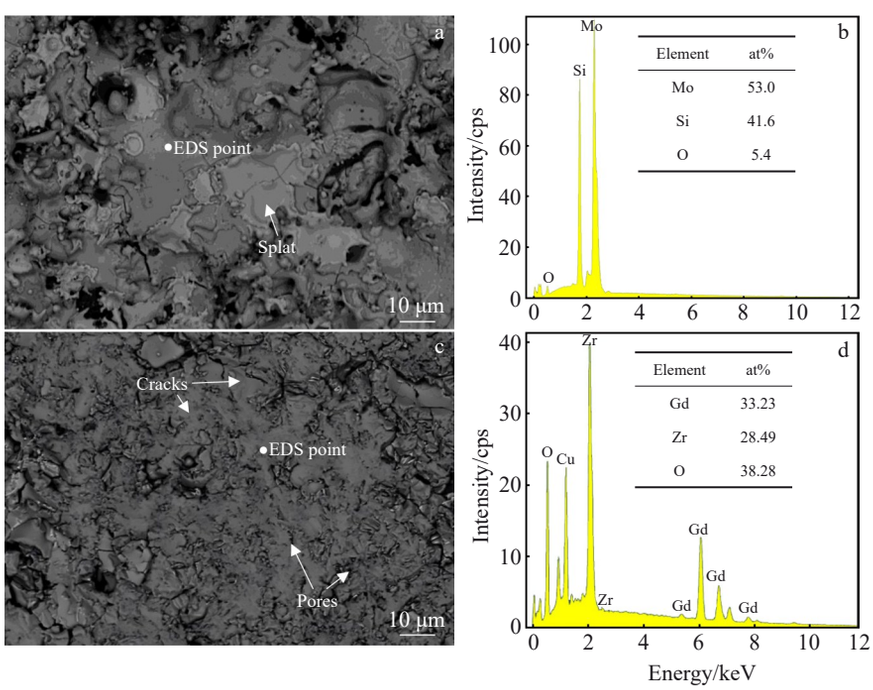

Fig.2 Microstructures (a, c) and EDS analysis results (b, d) of surface of $MoSi_2$ coating (a–b) and GZ coating (c–d)

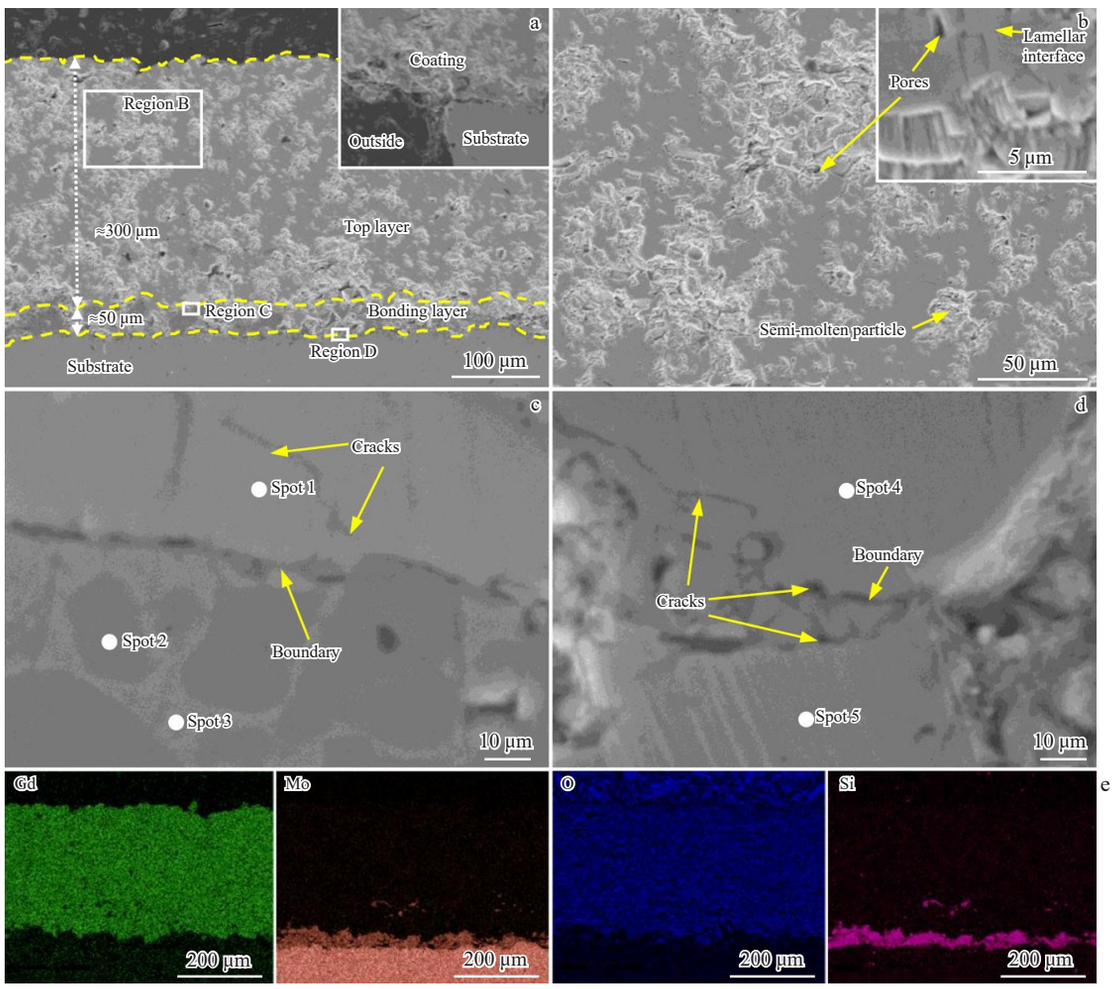

Fig.3 Cross-section microstructures of $MoSi_2$-GZ coating (a); magnified images of region B (b), region C (c), and region D (d) in Fig.3a; EDS element distributions corresponding to Fig.3a (e)

Table 3 Composition of spots marked in Fig.3 (at%)

Spot	Gd	Zr	O	Mo	Si
1	19.39	21.45	59.16	-	-
2	-	2.22	13.69	25.86	58.24
3	-	-	19.37	34.94	45.69
4	-	2.14	-	36.13	61.72
5	-	2.83	30.46	66.70	-

toughness calculation conditions in this study are consistent with those of the Evans & Wilshaw model, suggesting a correlation between anisotropic behavior and the accumulation of microvoids between thin films, which reduces the actual contact area. In APS-prepared coatings, micropores preferentially accumulate at the crack boundaries, forming the most susceptible regions to fracture[25]. Multiple and extensive cracking marks can also be observed near the coating surface and interface in the indentation region. This is related to cracks at the interface and influenced by the degree of particle melting at the surface interface[27]. Despite re-preheating and post-spray treatment during GZ coating preparation on the $MoSi_2$ layer to reduce thermal stress, it can

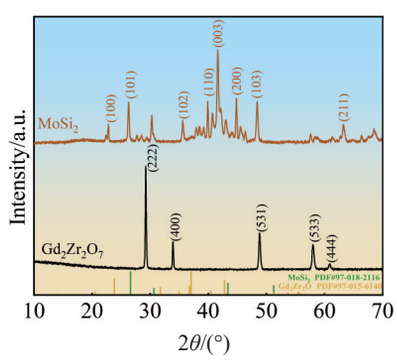

Fig.4 XRD patterns of $MoSi_2$ and GZ coatings on Mo-Re alloy

still be seen that the particle melting is affected, resulting in weak interlocking bonding[29].

The microhardness and fracture toughness of the $MoSi_2$-GZ composite coatings at different locations are shown in Fig. 6. Table 4 presents the relevant mechanical properties of the coating. As shown in Fig. 6a, it can be observed that most microhardness values of the coating are about 900 $HV_{0.2}$. The average microhardness is 883.3 $HV_{0.2}$. At the interface

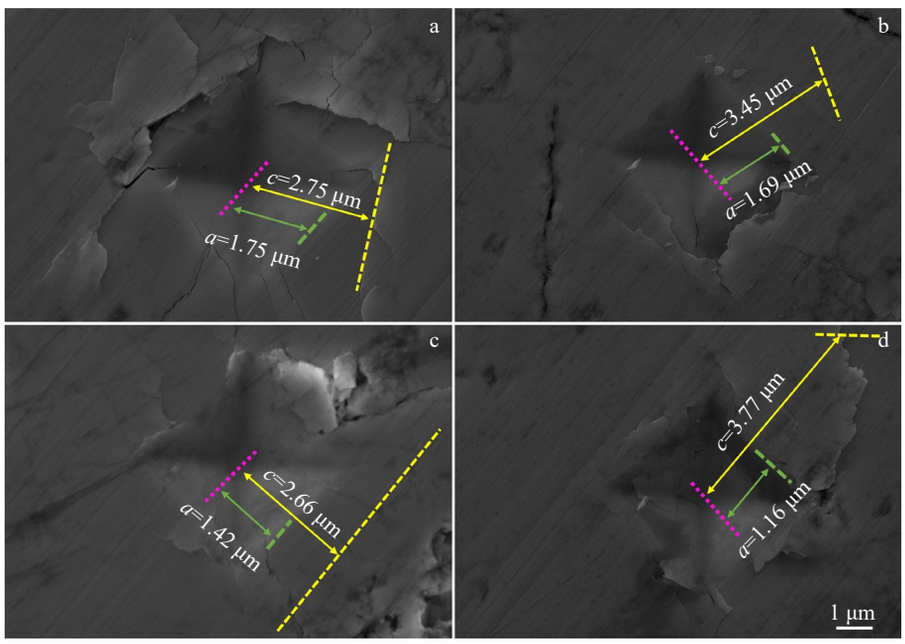

Fig.5 SEM images of microhardness indentation results on $MoSi_2$-GZ coating with different distances from surface: (a) 50 μm; (b) 100 μm; (c) 200 μm; (d) 300 μm

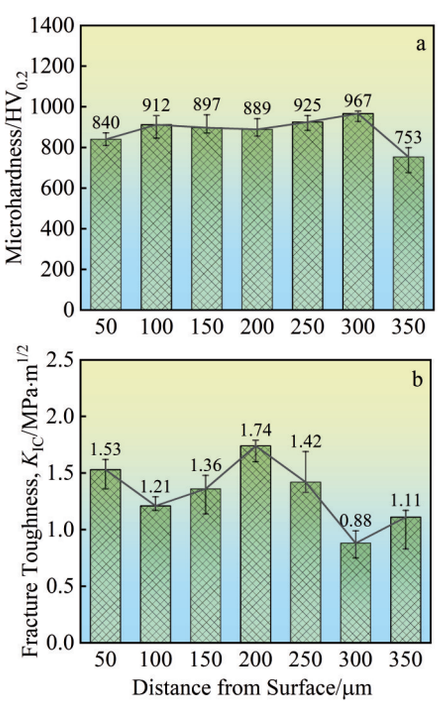

Fig.6 Microhardness (a) and fracture toughness (b) of $MoSi_2$-GZ coating

between $MoSi_2$ and GZ coatings, there is no significant variation in microhardness, indicating a lack of noticeable defects or pores at this interface. However, the fracture toughness of GZ and $MoSi_2$ coatings is 1.21 – 1.74 and 0.88 MPa·m$^{1/2}$, respectively, indicating weaker crack-propagation resistance in the $MoSi_2$ coating. Compared with that of $MoSi_2$ coating (0.88 MPa·m$^{1/2}$), the fracture toughness of GZ coating is higher (1.74 MPa·m$^{1/2}$), showing stronger resistance to crack propagation. There are two main reasons for the relatively lower fracture toughness of the $MoSi_2$ coatings: (1) a lower degree of melting leads to a reduction in anchor points for deposition splashing[16,28], which lowers bonding strength (the fracture occurs between $MoSi_2$ and GZ coatings rather than within the GZ coating), thus providing a pathway for crack propagation along the weak splashing boundaries; (2) an increase in porosity reduces the solid area carrying load and decreases the fracture toughness.

Table 4 Mechanical properties (thickness, porosity, bonding strength, and density) of Mo-Re sample with $MoSi_2$-GZ coating

Thickness/μm	Porosity/%	Bonding strength/MPa	Density/g·cm^{-3}
350	39	25	6.823

3.3 Thermal properties of $MoSi_2$-GZ coatings

The heat capacity of the $MoSi_2$-GZ coating is shown in Fig.7, which increases from 0.518 J·(K·g)$^{-1}$ to 0.601 J·(K·g)$^{-1}$ within the temperature of 800–1200 °C. The change in heat capacity is similar to that in the coefficient of thermal expansion: it rapidly increases at low temperatures and then becomes stable. This similarity can be attributed to its conformity with the Debye model[20] at low temperatures, where heat capacity is proportional to the cube of the temperature[17].

The thermal conductivity and thermal diffusivity of the $MoSi_2$-GZ coating are shown in Fig. 8. The insulation performance is related to the thermal conductivity of the coating. At 1200 °C, the composite coating exhibits a thermal

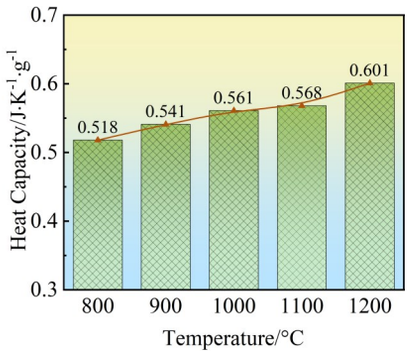

Fig.7 Heat capacity of $MoSi_2$-GZ coating

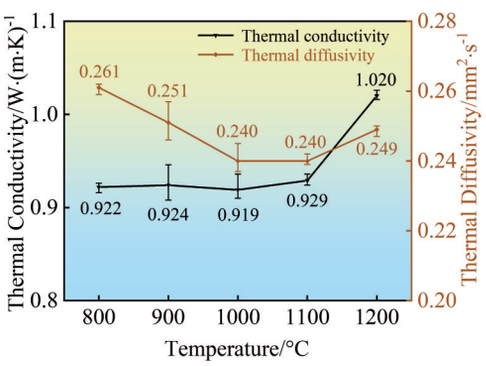

Fig.8 Thermal conductivity and thermal diffusivity of $MoSi_2$-GZ coating

conductivity of 1.020 $W\cdot(m\cdot K)^{-1}$, indicating good insulation properties for the $MoSi_2$-GZ composite coating. The low thermal conductivity of the $MoSi_2$-GZ composite coating is related to the phase composition and the high porosity (39%). For APS-prepared coating, the thermal conductivity of GZ is slightly increased with the increase in temperature from 800 °C to 1100 °C and significantly increased between 1100–1200 °C. Generally, lattice defects, such as vacancies, play a crucial role in the reduction of thermal conductivity[32]. Besides, oxygen vacancies are considered as the most essential lattice defects in ceramic materials, especially for the ceramics with strong insulation capabilities[33]. This result suggests that there are many oxygen vacancies in the GZ coating. In comparison, slight variation can be observed in the thermal diffusivity of the coating, and thermal diffusivity fluctuates between 0.240 – 0.261 mm^2/s. Briefly, the APS-prepared $MoSi_2$-GZ composite coating has high porosity (39%), low thermal conductivity (1.020 W/(m·K) at 1200 °C), low thermal diffusivity (0.249 mm^2/s at 1200 °C), and high oxygen vacancy concentration, resulting in low thermal diffusivity and thermal conductivity ratio, which ensures good insulation performance.

4 Conclusions

1) By selecting the composition of the dual-layer insulation coatings, the preparation process parameters and thickness of the composite coatings are determined. The $MoSi_2$-GZ composite coating exhibits high microhardness (883.3 $HV_{0.2}$) and good adhesion without apparent cracks at the interface.

2) The melting effect of particles and the presence of cracks at the interface affect the fracture toughness at the coating interface. Compared with that of $MoSi_2$ coating (0.88 $MPa\cdot m^{1/2}$), the fracture toughness of GZ coating is higher (1.74 $MPa\cdot m^{1/2}$), showing stronger resistance to crack propagation.

3) The APS-prepared $MoSi_2$-GZ composite coating has high porosity (39%), low thermal conductivity (1.020 W/m·K at 1200 °C), low thermal diffusivity (0.249 mm^2/s at 1200 °C), and high oxygen vacancy concentration, resulting in low thermal diffusivity and thermal conductivity ratio, which ensures good insulation performance.

References

1 Chang Tian, Gao Xuanqiao, Lin Xiaohui *et al*. *Rare Metal Materials and Engineering*[J], 2023, 52(1): 388 (in Chinese)
2 Xu Hailong, Huang Li, Zhang Wen *et al*. *Journal of Materials Research and Technology*[J], 2024, 30: 3877
3 Tyler D D, Valverde N A, Jodie A Y *et al*. *Materials & Design*[J], 2024, 244: 113226
4 Sun Lu, Li Mingjun, Chen Li *et al*. *Acta Materialia*[J], 2024, 278: 120270
5 Cheng Chunyu, Lv Tiantian, Song Bohao *et al*. *Surfaces and Interfaces*[J], 2024, 53: 105050
6 Hesamaldin A, Seyed A S, Arezoo S. *Surface and Coatings Technology*[J], 2024, 482: 130701
7 Shu Chaoxi, Wang Jinshuang, Lu Xianjun *et al*. *Journal of the European Ceramic Society*[J], 2024, 44(4): 2537
8 Zhao Hongxu, Deng Chunming, Fu Lang *et al*. *Surface Technology*[J], 2022, 51(2): 116
9 Mao Deng, Huang Zhangyi, Wang Haomin. *Scripta Materialia*[J], 2024, 242: 115945
10 Liu Xiangyang, Yu Yali, Han Yi *et al*. *Journal of the European Ceramic Society*[J], 2024, 44(15): 116736
11 Kadir M D, Abdullah C K, Yasin O *et al*. *Vacuum*[J], 2020, 177: 109401
12 Wang Haomin, Shi Yang, Deng Mao *et al*. *Ceramics International*[J], 2024, 50(17): 29268
13 Gao Yue, Guo Xiping, Qiao Yanqiang *et al*. *Corrosion Science*[J], 2019, 153: 283
14 Mao Jinyuan, Liu Min, Deng Chunming *et al*. *Rare Metal Materials and Engineering*[J], 2016, 45(6): 1386 (in Chinese)
15 Fu Wenbin, Dai Mingjiang, Wei Chunbei *et al*. *Rare Metal Materials and Engineering*[J], 2016, 45(10): 2543 (in Chinese)
16 Fu Tao, Zhang Yingyi, Shen Fuqiang *et al*. *Materials Characterization*[J], 2022, 192: 112192
17 Fu Tao, Han Zhichen, Zhang Yingyi *et al*. *International Journal of Refractory Metals and Hard Materials*[J], 2024, 124: 106831
18 Fu Tao, Zhang Yingyi, Chen Luyu *et al*. *Journal of Materials*

Research and Technology[J], 2024, 29: 491

19 Zhang Yingyi, Fu Tao, Yu Laihao *et al*. *Ceramics International*[J], 2022, 48: 20895

20 Alireza S, Mandana A, Mansour S. *Journal of Materials Research and Technology*[J], 2024, 30: 187

21 Zhang Yingyi, Yu Laiho, Fu Tao *et al*. *Surface and Coatings Technology*[J], 2022, 431: 128037

22 Zhang Yingyi, Yu Laihao, Fu Tao *et al*. *Journal of Alloys and Compounds*[J], 2022, 894: 162403

23 Lu Zhu, Zhang Shipeng, Ye Fan *et al*. *Composites Part B: Engineering*[J], 2024, 274: 111281

24 Sun Guoxun, Wang Weili, Sun Xiaoning. *Ceramics International*[J], 2022, 48(6): 8589

25 Shen Zaoyu, Liu Guanxi, Luo Yuqing *et al*. *Corrosion Science*[J], 2024, 226: 111641

26 Brenda J M F, Guilherme Y K, Siegfried A *et al*. *Additive Manufacturing Letters*[J], 2024, 9: 100206

27 Ji Shouchang, Li Jinglong, Yang Haiyu *et al*. *Rare Metal Materials and Engineering*[J], 2023, 52(10): 3345

28 Pan Yangyang, Han Dijuan, Huang Shansong *et al*. *Surface and Coatings Technology*[J], 2023, 468: 129715

29 Hesam R S, Mehdi S, Hossein E *et al*. *Surface and Coatings Technology*[J], 2017, 309: 959

30 Zois D A, Lekatou M V. *Surface and Coatings Technology*[J], 2009, 204: 15

31 Dong Lin, Liu Meijun, Zhang Xiaofeng *et al*. *Applied Surface Science*[J], 2021, 543: 148847

32 Wang Xin, Yang Tao, Li Qingyu *et al*. *Journal of the European Ceramic Society*[J], 2021, 41(4): 2415

33 Yao Shuwei, Li Changjiu, Tian Jiajia *et al*. *Acta Materialia*[J], 2016, 119: 9

Mo-Re合金表面$MoSi_2$和$Gd_2Zr_2O_7$复合涂层的显微组织和热性能

张　冲，汪　欣，徐海龙，李延超，马通祥，王少鹏

(西北有色金属研究院，陕西 西安 710016)

摘　要：在钼铼合金热端部件表面制备了超高温双层隔热涂层（TBCs），根据热膨胀系数及涂层功能设计并通过大气等离子喷涂技术完成了$MoSi_2$-$Gd_2Zr_2O_7$的双层TBCs的制备，并对其微观组织、力学性能及热学性能进行分析。结果表明：制备出的双层复合TBCs结合力良好，界面未出现明显裂纹。相较于$MoSi_2$涂层断裂韧性低（0.88 MPa·$m^{1/2}$），$Gd_2Zr_2O_7$涂层的断裂韧性更高（1.74 MPa·$m^{1/2}$），抗裂纹传播能力更强。制备的$MoSi_2$-$Gd_2Zr_2O_7$复合涂层孔隙率高（39%）、导热系数低（1.020 W·(m·K)$^{-1}$，1200 ℃）、热扩散系数低（0.249 mm^2/s，1200 ℃），氧空位浓度高，保证了良好的隔热性能。

关键词：$MoSi_2$-$Gd_2Zr_2O_7$涂层；钼铼合金；TBCs；隔热性能

作者简介：张　冲，男，1996年生，硕士，工程师，西北有色金属研究院，陕西 西安 710016，电话：029-86283410，E-mail：zhangchong0411@163.com